Supporting information

4,4',5,5'-Tetracarboxy-2,2'-Bipyridine Ru(II) Sensitizers for Dye-Sensitized Solar Cells

Chun-Cheng Chou,[a] Fa-Chun Hu,[a] Kuan-Lin Wu,[a] Tainan Duan,[a] Yun Chi,*[,a] Shih-Hung Liu,[b] Gene-Hsiang Lee,[b] Pi-Tai Chou*[,b]

[a] Department of Chemistry and Low Carbon Energy Research Center, National Tsing Hua University, Hsinchu 30013, Taiwan; E-mail: ychi@mx.nthu.edu.tw

[b] Department of Chemistry and Center for Emerging Material and Advanced Devices, National Taiwan University, Taipei 10617, Taiwan; E-mail: chop@ntu.edu.tw

Experimental section

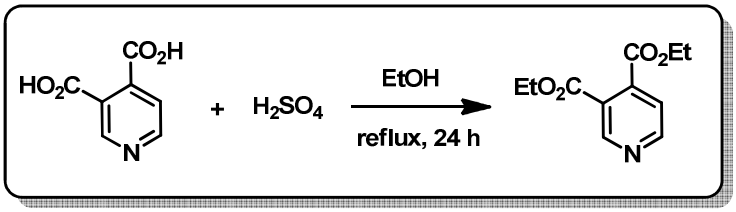

Synthesis of 3,4-di-ethoxycarbonyl pyridine:

The ethanol solution of cinchomeronic acid (10.0 g, 59.8 mmol) was added concentrate H_2SO_4 (12 mL) slowly, and the mixture was heated to reflux for 2 days. After cooling the reaction mixture to RT, excess of EtOH was first stripped off. After then, the oily mixture was dissolved in ethyl acetate, neutralized with $NH_4OH_{(aq)}$, dried over Na_2SO_4 and concentrated. Finally, the product was purified by silica gel column chromatography (ethyl acetate : hexane = 1 : 3). Yield: 9.0 g, 67%.

Selected spectral data: ^{1}H NMR (400 MHz, $CDCl_3$, 298 K): δ 9.04 (s, 1H), 8.79 (d, J_{HH} = 5.2 Hz, 1H), 7.47 (d, J_{HH} = 5.2 Hz, 1H), 4.41 ~ 4.35 (m, 4H), 1.38 ~ 1.34 (m, 6H).

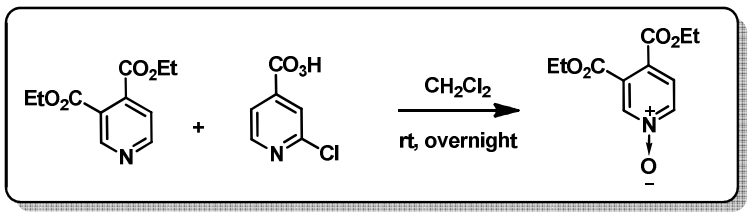

Synthesis of 3,4-di-ethoxycarbonyl-pyridine 1-oxide:

mCPBA (11.0 g, 63.7 mmol) was dissolved in CH_2Cl_2 (100 mL) and slowly added into the CH_2Cl_2 solution (150 mL) of 3,4-di-ethoxycarbonyl pyridine (9.0 g, 40.3

mmol). The mixture was stirred at room temperature overnight, the resultant solution was quenched by $Na_2CO_{3(aq)}$, thoroughly washed with deionized water and dried over anhydrous Na_2SO_4. Finally, the organic layer was concentrated using a rotary evaporator, and the residue was used for subsequent reaction without purification. Yield: 8.9 g, 92.3%.

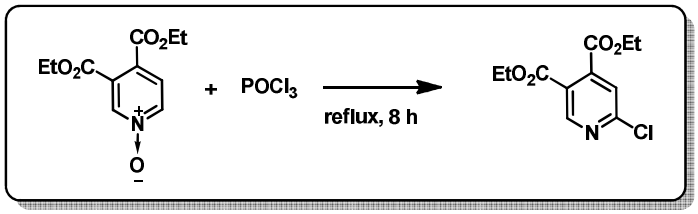

Synthesis of 6-chloro-3,4-di-ethoxycarbonyl pyridine:

3,4-di-ethoxycarbonyl-pyridine 1-oxide (9.2 g, 38.5 mmol) was dissolved in $POCl_3$ (110 mL) and was heated to reflux overnight. The $POCl_3$ was removed under vacuum, and the residue was dissolved in CH_2Cl_2, washed with $Na_2CO_{3(aq)}$, and dried over anhydrous Na_2SO_4. Finally, the organic layer was concentrated using a rotary evaporator, and the crude product was purified by column chromatography on silica gel. Yield: 5.3 g, 54%.

Selected spectral data: ^{1}H NMR (400 MHz, $CDCl_3$, 298 K): δ 8.83 (s, 1H), 7.48 (s, 1H), 4.40 ~ 4.36 (m, 4H), 1.38 ~ 1.34 (m, 6H).

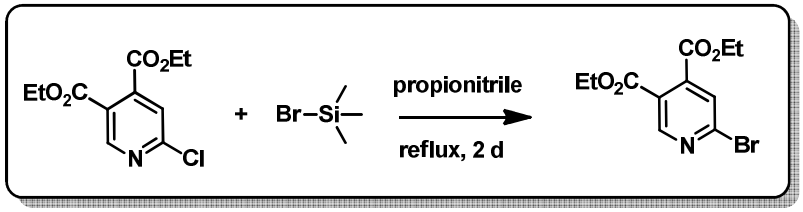

Synthesis of 6-bromo-3,4-di-ethoxycarbonyl-pyridine:

6-Chloro-3,4-di-ethoxycarbonyl pyridine (5 g, 19.4 mmol) was dissolved in propionitrile (60 mL), and bromotrimethylsilane (17.8 g, 116.4 mmol) was slowly added. The mixture was heated to reflux for 2 days, followed by removal of solvent under vacuum. Subsequently, the residue was dissolved in CH_2Cl_2 and the solution was washed with $Na_2CO_{3(aq)}$, dried over anhydrous Na_2SO_4, and concentrated using a rotary evaporator. Finally, the residue was purified by silica gel column chromatography (ethyl acetate : hexane = 1 : 5). Yield: 4.1 g, 70%.

Selected spectral data: ^{1}H NMR (400 MHz, $CDCl_3$, 298 K): δ 8.79 (s, 1H), 7.64 (s, 1H), 4.42 ~ 4.35 (m, 4H), 1.38 ~ 1.35 (m, 6H).

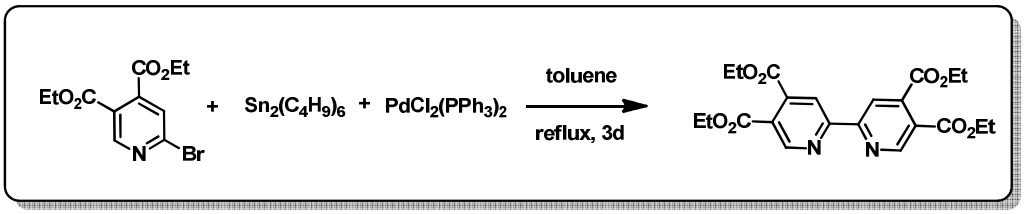

Synthesis of 4,4',5,5'-tetra-ethoxycarbonyl-2,2'-bipyridine:

A toluene solution (30 mL) of 6-bromo-3,4-di-ethoxycarbonyl pyridine (2.0 g, 6.6 mmol), $Sn_2(C_4H_9)_6$ (4.22 g, 7.3 mmol), and $PdCl_2(PPh_3)_2$ (0.23 g, 0.3 mmol) was refluxed for 3 days. After cooling the solution to RT, toluene was removed under vacuum, and the residue was purified by silica gel column chromatography (ethyl acetate : hexane = 1 : 3). Yield: 0.65 g, 44%.

Selected spectral data: MS (EI): m/z 444.1 $(M)^+$. ^1H NMR (400 MHz, $CDCl_3$, 298 K): δ 9.12 (s, 2H), 8.65 (s, 2H), 4.46 ~ 4.39 (m, 8H), 1.42 ~ 1.37 (m, 12H).

Computational Method

All calculations were performed by Gaussian 09 program.[S1] The ground state structures of TCR-1 and TCR-2 were first optimized with density functional theory (DFT) at B3LYP/LANL2DZ (Ru) and 6-31G* (H, C, N, O, F, S) level. The optimized structures were then used to calculate 60 lowest singlet energy optical excitations using the time-dependent density functional theory (TDDFT) method. Their lowest ground triplet state energies were also calculated. To mimic the solution environment a polarizable continuum model (PCM) in Gaussian 09 was applied using dimethylformamide (DMF) as the solvent.

In order to investigate the behavior of the Ru(II) dyes adsorbing onto the TiO_2 surface, we also simulated TFRS-2, TFRS-52, TCR-1 and TCR-2 anchoring onto the anatase (101) TiO_2 surface. We have reported the computation of black dye (N749) anchoring onto the $(TiO_2)_{28}$ surface[S2]. In this study, we then extended to a larger surface using $(TiO_2)_{38}$ nanocluster as the simulation model. The surface area of $(TiO_2)_{38}$ was suitable for both the dicarboxy groups to anchor onto. In this approach the ground state structures of TFRS-2/$(TiO_2)_{38}$, TFRS-52/$(TiO_2)_{38}$, TCR-1/$(TiO_2)_{38}$ and TCR-2/$(TiO_2)_{38}$ were optimized at B3LYP/LANL2DZ (Ti, Ru) and 6-31G* (H, C, N, O, F, S) level and DMF was used as the solvent.

Photovoltaic characterization

Photovoltaic performances were recorded under a class-AAA solar simulator (Model 11016A, Sun 3000, ABET Technologies) equipped with a 550 W xenon light source and water-cooling stage (25 °C). The output power density (100 mW/cm^2) was calibrated using a certificated KG-3 Si reference cell and with a circular aperture of 8

mm. The current-voltage characteristic was obtained with a 4-wire setup, with delay time of 100 ms and bias scan mode switching from short-circuit to open-circuit using a Keithley digital source meter (Model 2400). The incident photon-to-current conversion efficiency (IPCE) was calculated with the equation $1240 \cdot J_{SC}(\lambda)/(\lambda \cdot P_{in}(\lambda))$, where J_{SC} is the short-circuit current density under monochromatic illumination in unit of A/cm^2, λ is the wavelength of incident monochromatic light in unit of nanometer, and P_{in} is the monochromatic light intensity in unit of W/cm^2, and were plotted as a function of incident wavelength with an increment of 10 nm. The current was pre-amplified by a current amplifier (SR570) and measured using a Keithley 2400 source meter. It should be noted that 10 values of J_{SC} (in interval of 50 ms) were collected sequentially after illuminating the device for 3 seconds and then averaged for calculation of IPCE. A 300 W Xe lamp (Model 6258, Newport Oriel) combined with an Oriel cornerstone 260 1/4 m monochromator (Model 74100) provided the monochromatic beam (dc mode). The beam power intensity was calibrated with a power meter (Model 1936-C, Newport) equipped with a Newport 818-UV photodetector.

Electrochemical study

Cyclic voltammetry was measured using an electrochemical analyzer (CH Instrument) and a single-compartment, three-electrode cell with a Pt wire counter electrode. The studied sensitizers were dissolved in mixed DMSO and ethanol, and adsorbed on a transparent TiO_2 film (*ca.* 7 μm) which served as the working electrode, while Ag/AgCl electrode and 0.1 M of $TBAPF_6$ (TBA = NBu_4^+) in acetonitrile were employed as the reference electrode and supporting electrolyte, respectively. The obtained data was calibrated with Fc/Fc^+ reference and then converted to value relative to NHE by addition of 0.63 V.[S3]

Charge extraction and intensity-modulated photovoltage spectroscopy

Charge extraction (CE) was measured with the PGSTAT302N electrochemical workstation (Autolab) at an open-circuit condition for the photovoltage of the device to attain a steady state; the red light-emitting diode (LED, 627 nm) was then terminated while the device simultaneously switched to a short-circuit condition to measure the excess charges generated in the film.[S4,5] Intensity-modulated photovoltage spectroscopy (IMVS) measurement was conducted using the same PGSTAT302N electrochemical workstation equipped with a frequency response analyzer (FRA) to drive a red light emitting diode. The analysis of the photovoltage response of the cells was conducted in the frequency range of 10^4 – 1 Hz and LED supplied the AC (modulation depth 10%) perturbation current superimposed on the

DC current.

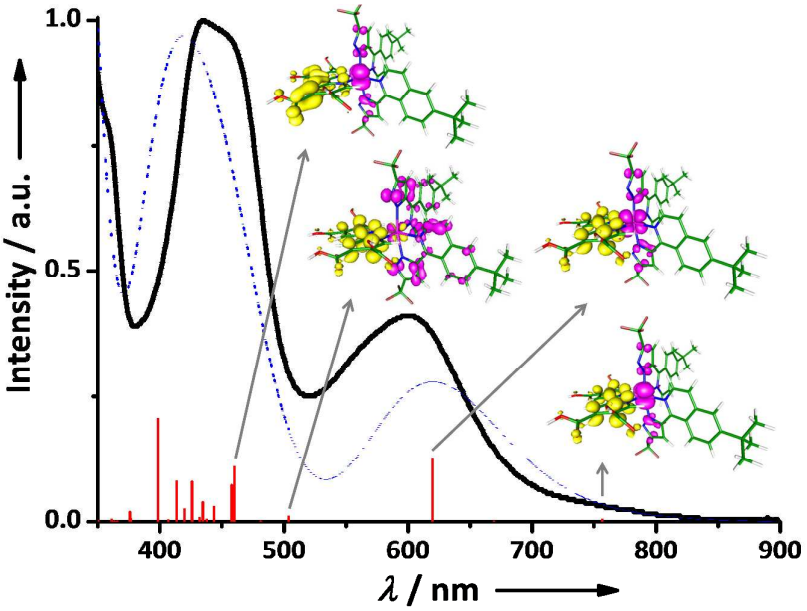

Figure S1. Experimental (black line) and TDDFT calculated (blue dashed line obtained with a Gaussian convolution σ = 0.2 eV) absorption spectra of TCR-2 in DMF. Also depicted are the TDDFT calculated absorption wavelengths (red vertical lines) and the relative transition probability (magnitude of vertical lines). Selected frontier orbitals (pink: occupied orbital, yellow: unoccupied orbital) that contribute to the major transitions are also shown.

Table S1. The wavelengths, transition probabilities and charge transfer character of the optical transitions over 300 nm in selected states with oscillator strength > 0.03 for for **TCR-1** in DMF. The lowest triplet optical transition ($S_0 \rightarrow T_1$) is also listed.

State	λ_{cal} (nm)	f	Assignments	MLCT
T_1	857.2	0	HOMO-1→LUMO(92%)	42.93%
S_1	759.7	0.0039	HOMO→LUMO(97%)	56.45%
S_3	606.8	0.1307	HOMO-1→LUMO(90%) HOMO→LUMO+1(6%)	45.86%
S_6	458.4	0.1577	HOMO→LUMO+1(63%) HOMO-5→LUMO(8%) HOMO-4→LUMO(7%)	39.91%
S_8	452.9	0.03	HOMO-2→LUMO+1(59%) HOMO-1→LUMO+1(18%) HOMO-3→LUMO(11%)	38.94%
S_{14}	416.7	0.16	HOMO-1→LUMO+2(83%)	44.52%
S_{18}	398.6	0.4128	HOMO-2→LUMO+3(86%) HOMO-2→LUMO+2(5%)	46.77%
S_{19}	372.5	0.1555	HOMO-2→LUMO+4(63%) HOMO-9→LUMO(13%)	31.35%
S_{27}	337.4	0.1361	HOMO-5→LUMO+2(35%) HOMO-5→LUMO+3(18%) HOMO-2→LUMO+6(10%) HOMO-3→LUMO+4(9%) HOMO-4→LUMO+2(8%)	6.04%
S_{29}	334	0.1006	HOMO-11→LUMO(19%) HOMO-4→LUMO+3(17%) HOMO-3→LUMO+3(14%) HOMO→LUMO+5(12%) HOMO-4→LUMO+2(12%)	7.61%
S_{41}	323.3	0.1079	HOMO-1→LUMO+5(39%) HOMO-12→LUMO(32%) HOMO→LUMO+14(6%)	20.38%
S_{42}	320.2	0.5914	HOMO-3→LUMO+4(52%) HOMO-2→LUMO+6(11%) HOMO-3→LUMO+3(8%) HOMO-4→LUMO+4(7%) HOMO-12→LUMO(7%)	3.11%
S_{43}	319.1	0.0883	HOMO-1→LUMO+6(36%) HOMO-3→LUMO+3(36%) HOMO-4→LUMO+3(13%)	19.24%
S_{44}	317.6	0.1479	HOMO-1→LUMO+6(45%) HOMO-3→LUMO+3(16%) HOMO→LUMO+7(13%)	32.76%
S_{45}	316.1	0.1696	HOMO-12→LUMO(27%) HOMO-1→LUMO+5(24%) HOMO→LUMO+7(21%)	25.48%
S_{46}	315.9	0.1373	HOMO→LUMO+7(42%) HOMO-1→LUMO+5(13%) HOMO-12→LUMO(12%)	34.20%
S_{48}	312.5	0.0738	HOMO-2→LUMO+6(47%) HOMO-4→LUMO+4(16%) HOMO-5→LUMO+3(7%) HOMO-6→LUMO+3(6%)	26.29%

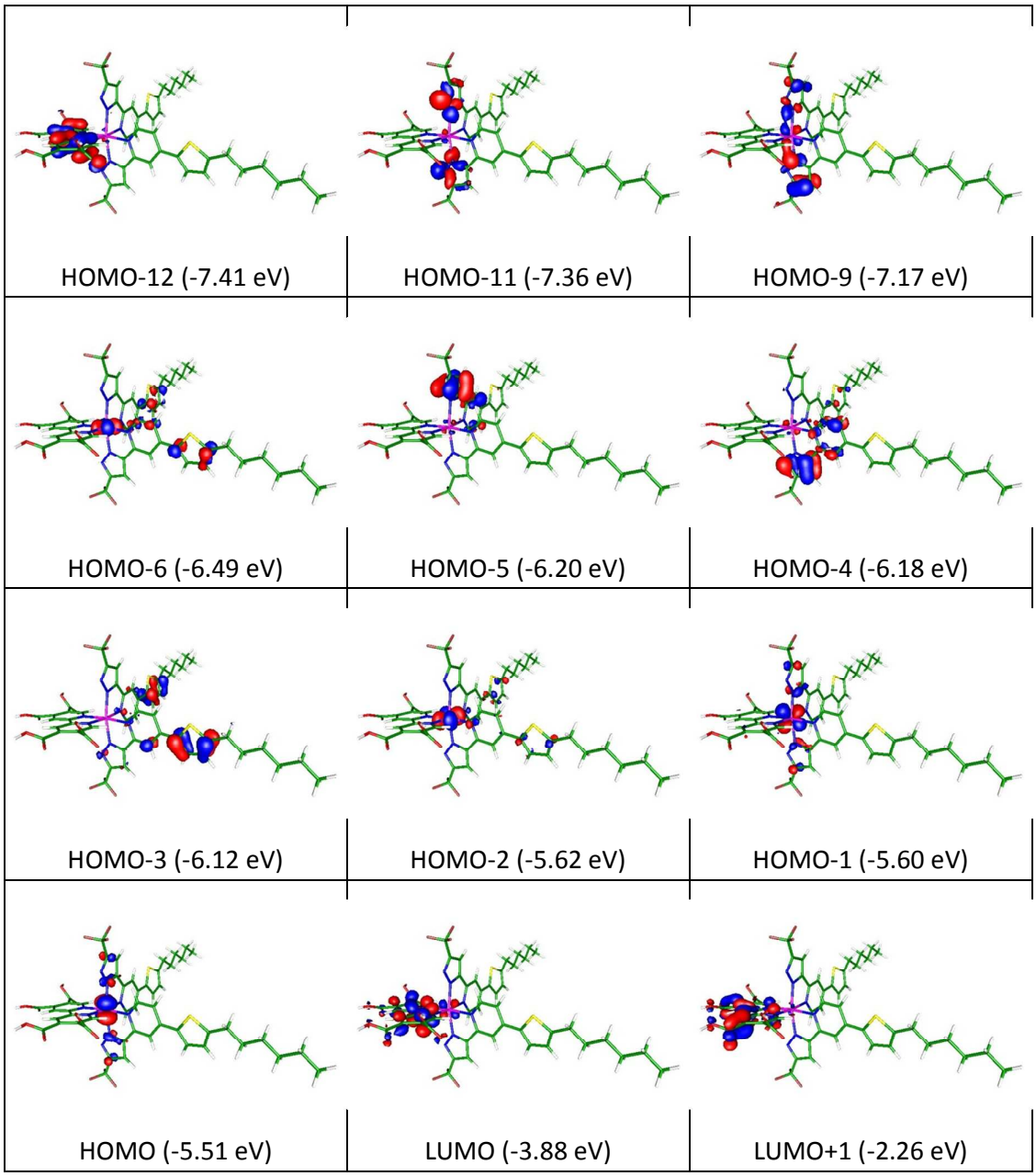

Figure S2-1. Frontier molecular orbitals pertinent to the optical transitions for **TCR-1**.

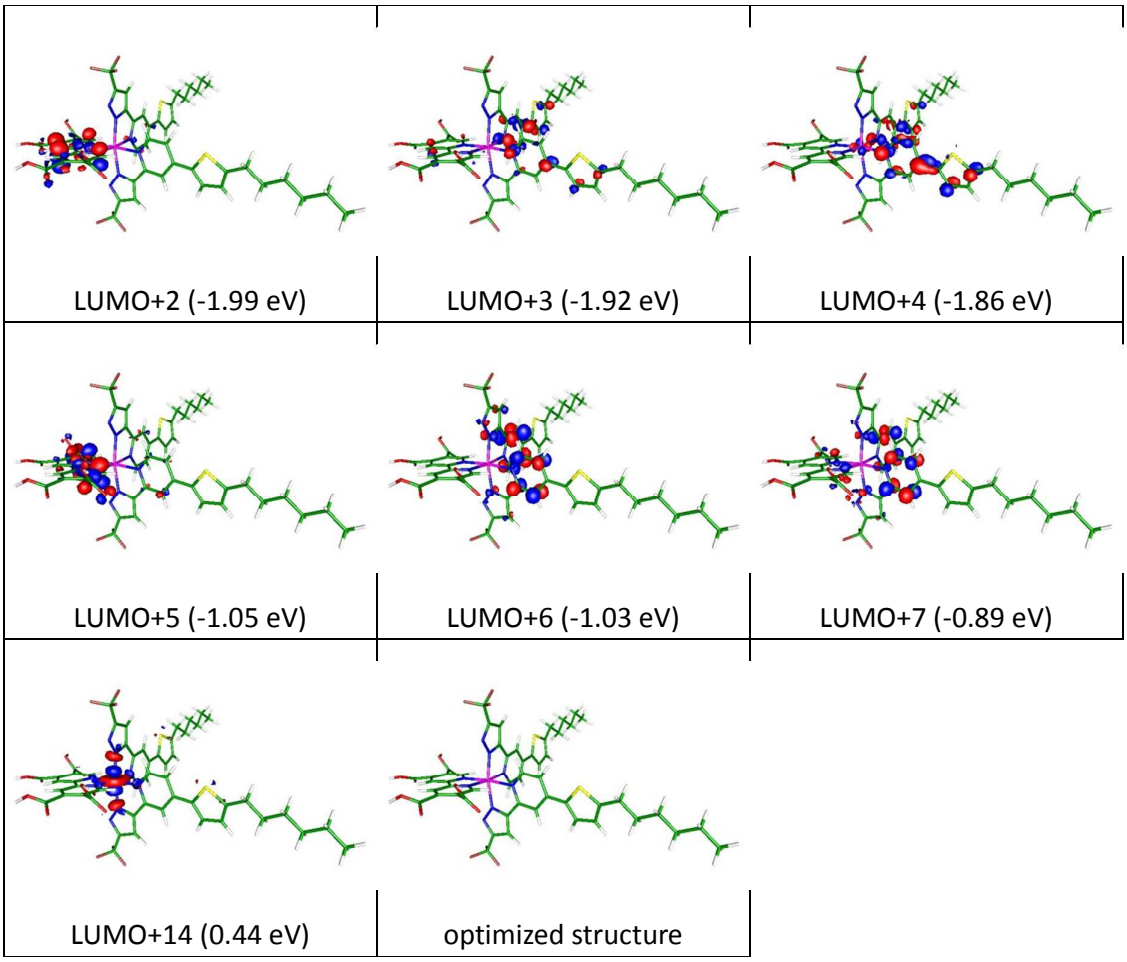

Figure S2-2. Frontier molecular orbitals pertinent to the optical transitions for **TCR-1**. For the clarity of viewing, the optimized structure with no involvement of frontier orbitals is shown at the last figure.

Table S2. The wavelengths, transition probabilities and charge transfer character of the optical transitions over 300 nm in selected states with oscillator strength > 0.01 for for **TCR-2** in DMF. The lowest triplet optical transition ($S_0 \rightarrow T_1$) is also listed.

State	λ_{cal} (nm)	*f*	Assignments	MLCT
T_1	876.2	0	HOMO-1→LUMO(92%)	39.29%
S_1	756.8	0.0033	HOMO→LUMO(97%)	55.73%
S_3	619.7	0.1252	HOMO-1→LUMO(93%)	39.72%
S_4	503.6	0.01	HOMO-3→LUMO(93%) HOMO→LUMO+1(6%)	3.87%
S_6	460.1	0.1079	HOMO→LUMO+1(73%) HOMO-1→LUMO+1(6%)	38.58%
S_7	457.9	0.0724	HOMO-1→LUMO+1(85%) HOMO→LUMO+1(5%)	44.69%
S_{12}	425.7	0.0794	HOMO-1→LUMO+2(60%) HOMO-1→LUMO+3(35%)	46.62%
S_{14}	413.6	0.08	HOMO-1→LUMO+3(50%) HOMO-1→LUMO+2(25%) HOMO-2→LUMO+4(12%)	42.89%
S_{16}	398.2	0.2053	HOMO-2→LUMO+3(86%) HOMO-2→LUMO+2(6%)	50.37%
S_{25}	341.5	0.0717	HOMO-8→LUMO(57%) HOMO-11→LUMO(13%) HOMO-10→LUMO(7%)	-5.02%
S_{26}	340.4	0.0526	HOMO-3→LUMO+4(41%) HOMO-7→LUMO(7%) HOMO-8→LUMO(7%) HOMO→LUMO+11(6%)	3.54%
S_{28}	337.2	0.0663	HOMO-4→LUMO+2(65%) HOMO-3→LUMO+4(7%) HOMO-2→LUMO+11(5%)	16.18%
S_{29}	334.8	0.1581	HOMO-4→LUMO+3(75%) HOMO-4→LUMO+2(9%)	17.90%
S_{30}	331	0.0785	HOMO-4→LUMO+4(72%) HOMO-11→LUMO(7%)	13.47%
S_{32}	327.6	0.0405	HOMO-1→LUMO+5(36%) HOMO→LUMO+14(16%) HOMO-11→LUMO(8%) HOMO-4→LUMO+4(6%) HOMO-1→LUMO+11(5%)	21.58%
S_{33}	327.2	0.0429	HOMO-10→LUMO(33%) HOMO-8→LUMO(15%) HOMO-11→LUMO(14%) HOMO-4→LUMO+4(6%) HOMO-1→LUMO+5(6%) HOMO→LUMO+5(5%)	4.39%
S_{34}	322.7	0.1348	HOMO→LUMO+14(22%) HOMO-1→LUMO+5(20%) HOMO-11→LUMO(13%) HOMO-10→LUMO(8%) HOMO-1→LUMO+11(7%)	12.87%
S_{37}	318.7	0.0606	HOMO→LUMO+6(88%)	56.87%
S_{38}	316.1	0.2708	HOMO-1→LUMO+5(31%) HOMO-10→LUMO(28%) HOMO-11→LUMO(19%)	14.52%
S_{45}	302.8	0.2934	HOMO-2→LUMO+6(79%) HOMO-1→LUMO+7(9%)	48.77%

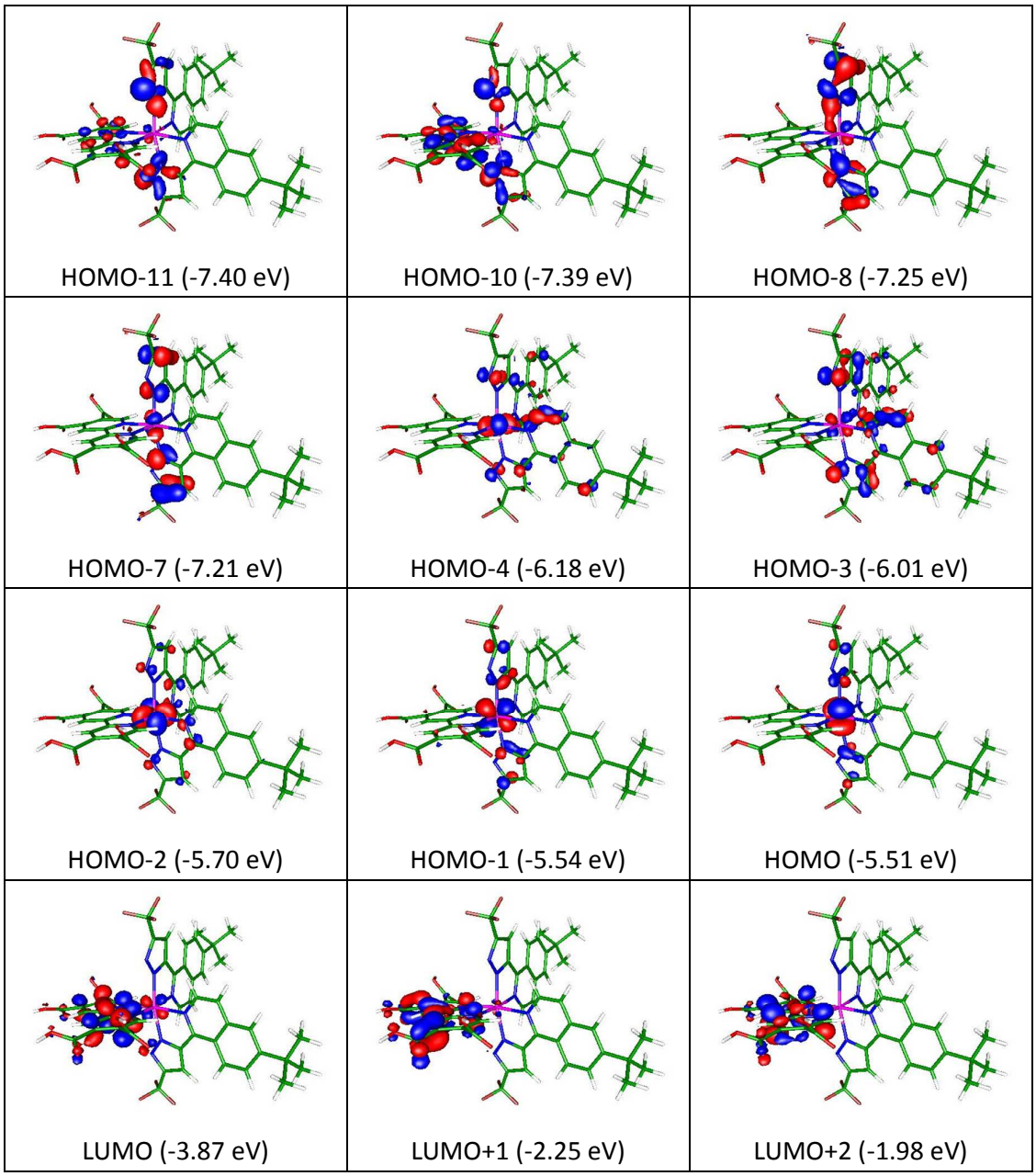

Figure S3-1. Frontier molecular orbitals pertinent to the optical transitions for **TCR-2**.

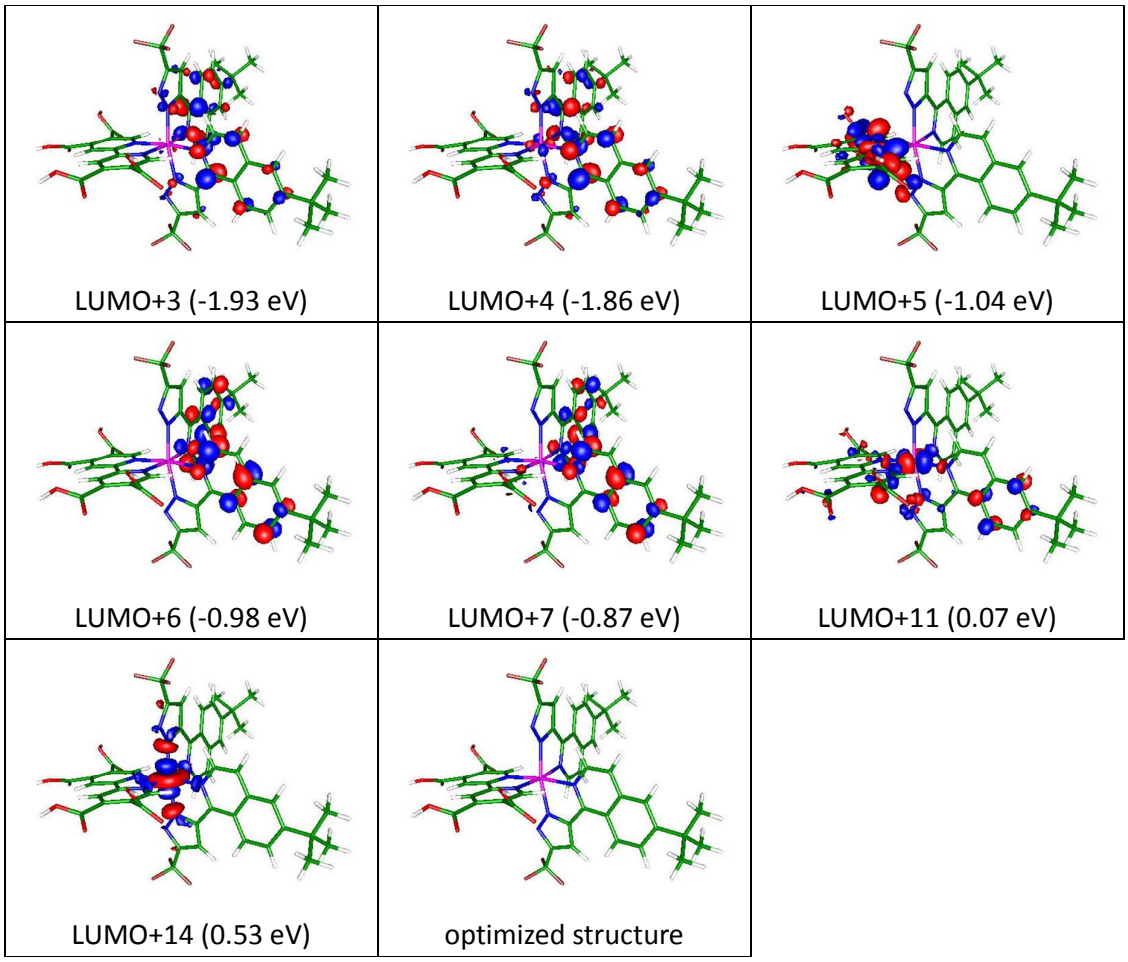

Figure S3-2. Frontier molecular orbitals pertinent to the optical transitions for **TCR-2**. For the clarity of viewing, the optimized structure with no involvement of frontier orbitals is shown at the last figure.

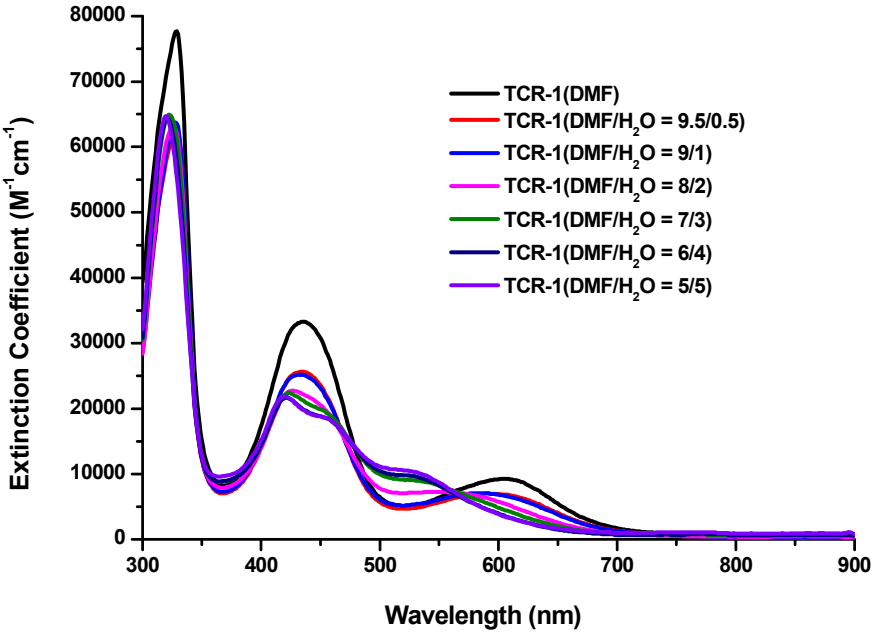

Figure S4. UV-Vis absorption spectra of Ru(II) sensitizers at 1×10^{-5} M in DMF and in mixed solvent with various H_2O content.

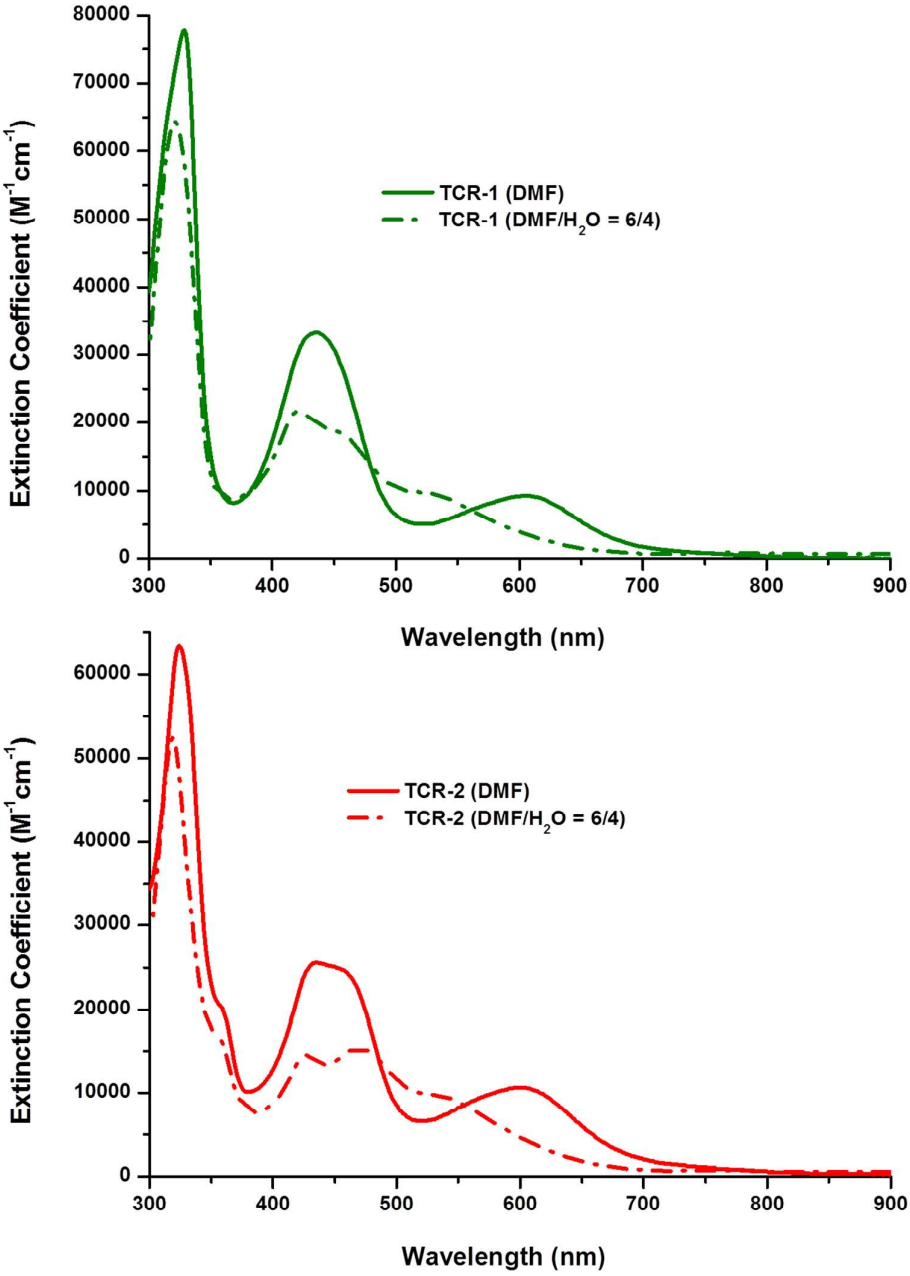

Figure S5. UV-Vis absorption spectra of Ru(II) sensitizers at 1×10^{-5} M in DMF and in mixed solvent (DMF/H_2O=6/4).

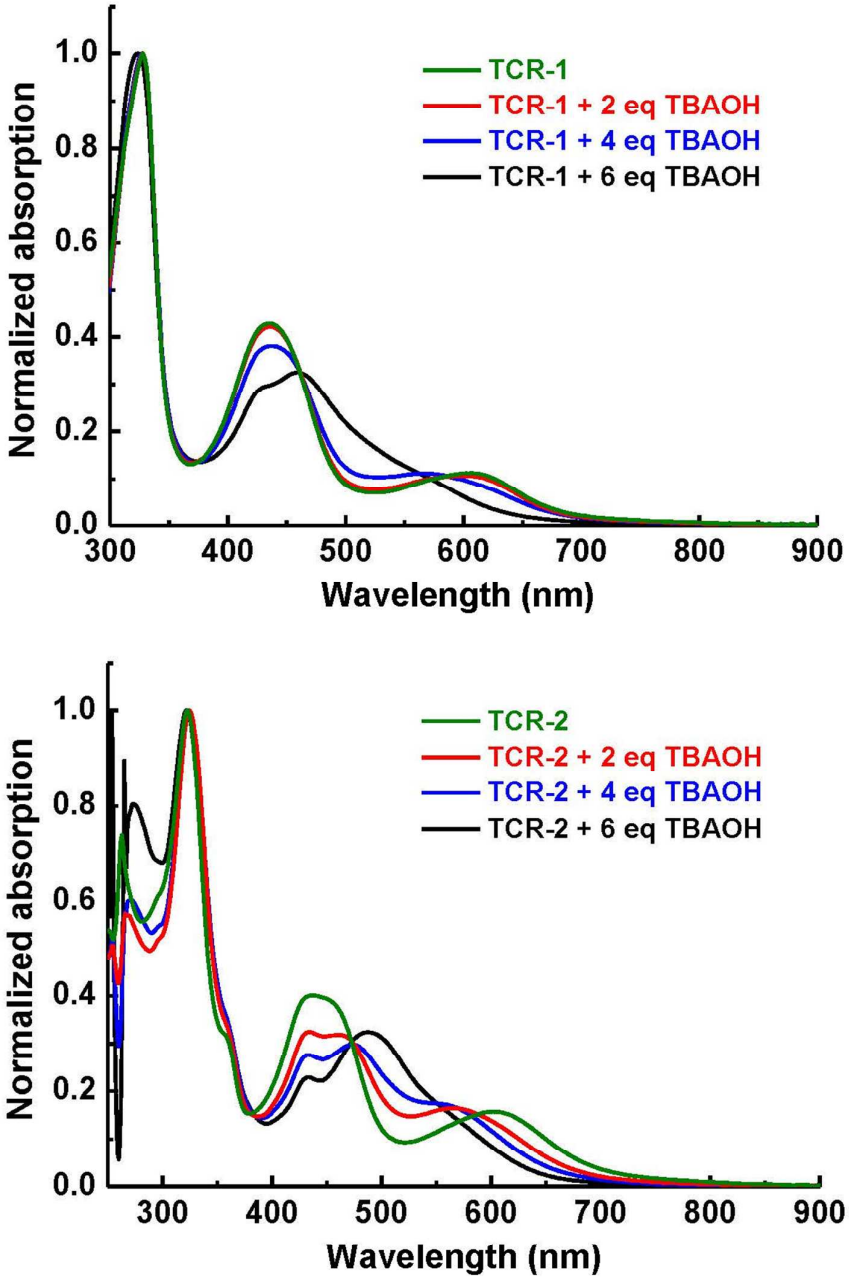

Figure S6. UV-Vis absorption spectra of Ru(II) sensitizers TCR-2 and TCR-2 at 1.0×10^{-4} M in DMF added with various amount of methanol solution containing TBAOH at 1.0×10^{-2} M.

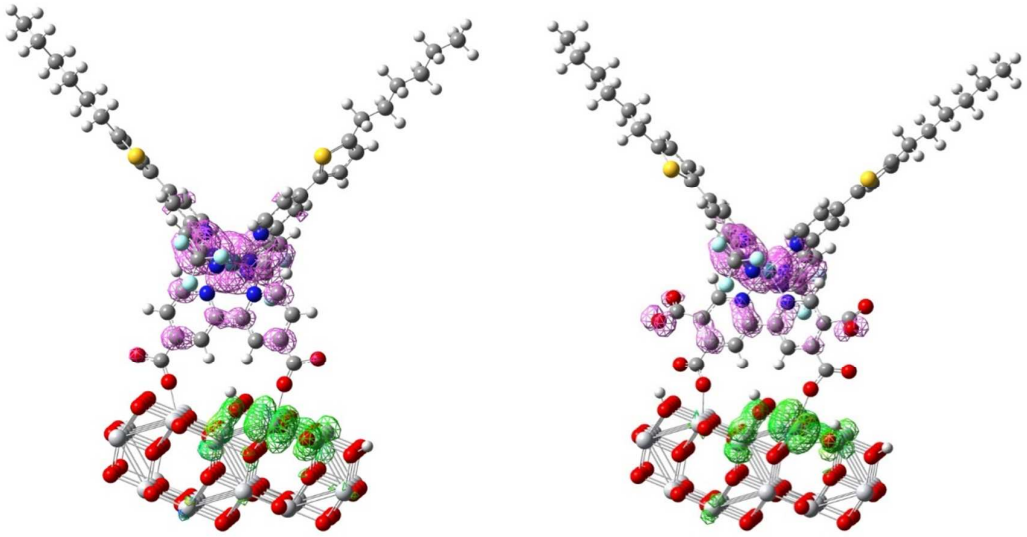

(a) TFRS-2/$(TiO_2)_{38}$ (b) TRC-1/$(TiO_2)_{38}$

Figure S7. The frontier molecular orbitals HOMO (pink mesh) and LUMO (green mesh) of a) TFRS-2/$(TiO_2)_{38}$ (left) and b) TCR-1/$(TiO_2)_{38}$ (right).

Reference

S1. Frisch, M. J.; Trucks, G. W.; Schlegel, H. B.; Scuseria, G. E.; Robb, M. A.; Cheeseman, J. R.; Scalmani, G.; Barone, V.; Mennucci, B.; Petersson, G. A.; Nakatsuji, H.; Caricato, M.; Li, X.; Hratchian, H. P.; Izmaylov, A. F.; Bloino, J.; Zheng, G.; Sonnenberg, J. L.; Hada, M.; Ehara, M.; Toyota, K.; Fukuda, R.; Hasegawa, J.; Ishida, M.; Nakajima, T.; Honda, Y.; Kitao, O.; Nakai, H.; Vreven, T.; Montgomery, J. A.; Peralta, J. E.; Ogliaro, F.; Bearpark, M.; Heyd, J. J.; Brothers, E.; Kudin, K. N.; Staroverov, V. N.; Kobayashi, R.; Normand, J.; Raghavachari, K.; Rendell, A.; Burant, J. C.; Iyengar, S. S.; Tomasi, J.; Cossi, M.; Rega, N.; Millam, J. M.; Klene, M.; Knox, J. E.; Cross, J. B.; Bakken, V.; Adamo, C.; Jaramillo, J.; Gomperts, R.; Stratmann, R. E.; Yazyev, O.; Austin, A. J.; Cammi, R.; Pomelli, C.; Ochterski, J. W.; Martin, R. L.; Morokuma, K.; Zakrzewski, V. G.; Voth, G. A.; Salvador, P.; Dannenberg, J. J.; Dapprich, S.; Daniels, A. D.; Farkas; Foresman, J. B.; Ortiz, J. V.; Cioslowski, J.; Fox, D. J. *Gaussian 09, Revision A.1; Gaussian Inc.* **2009**, Wallingford, CT.

S2. Liu, S.-H.; Fu, H.; Cheng, Y.-M.; Wu, K.-L.; Ho, S.-T.; Chi, Y.; Chou, P.-T. *J. Phys. Chem. C*, **2012**, *116*, 16338.

S3. Pavlishchuk, V. V.; Addison, A. W. *Inorg. Chim. Acta*, **2000**, *298*, 97.

S4. Duffy, N. W.; Peter, L. M.; Rajapakse, R. M. G.; Wijayantha, K. G. U. *Electrochem. Commun.*, **2000**, *2*, 658.

S5. Bailes, M.; Cameron, P. J.; Lobato, K.; Peter, L. M. *J. Phys. Chem. B*, **2005**, *109*, 15429.